Check for updates

AGU ADVANCING EARTH AND SPACE SCIENCE

Geophysical Research Letters

RESEARCH LETTER
10.1029/2020GL090041

Special Section:
The COVID-19 Pandemic: Linking Health, Society and Environment

Abnormally Shallow Boundary Layer Associated With Severe Air Pollution During the COVID-19 Lockdown in China

Tianning Su[1], Zhanqing Li[1], Youtong Zheng[1], Qingzu Luan[1,2], and Jianping Guo[3]

[1]Department of Atmospheric and Oceanic Sciences and ESSIC, University of Maryland, College Park, MD, USA, [2]Beijing Municipal Climate Center, Beijing, China, [3]State Key Laboratory of Severe Weather, Chinese Academy of Meteorological, Sciences, Beijing, China

Abstract After the 2020 Lunar New Year, the Chinese government implemented a strict nationwide lockdown to inhibit the spread of the Coronavirus Disease 2019 (COVID-19). Despite the abrupt decreases in gaseous emissions caused by record-low anthropogenic activities, severe haze pollution occurred in northern China during the COVID lockdown. This paradox has attracted the attention of both the public and the scientific community. By analyzing comprehensive measurements of air pollutants, planetary boundary layer (PBL) height, and surface meteorology, we show that the severe air pollution episode over northern China coincided with the abnormally low PBL height, which had reduced by 45%, triggering strong aerosol-PBL interactions. After dynamical processes initiated the temperature inversion, the Beijing metropolitan area experienced a period with continuously shallow PBLs during the lockdown. This unprecedented event provided an experiment showcasing the role of meteorology, in particular aerosol-PBL interactions in affecting air quality.

Key Points:
- Based on nationwide observations, variations in air pollution and meteorology are discussed during the COVID lockdown
- The severe air pollution during the lockdown coincided with abnormally shallow PBL triggering strong aerosol-PBL interactions
- Beijing experienced a period with continuously shallow PBLs initiated by dynamical processes, which warrant the formation of haze event

Supporting Information:
- Supporting Information S1

Correspondence to:
T. Su and Z. Li,
tianning@umd.edu;
zli@atmos.umd.edu

Citation:
Su, T., Li, Z., Zheng, Y., Luan, Q., & Guo, J. (2020). Abnormally shallow boundary layer associated with severe air pollution during the COVID-19 lockdown in China. *Geophysical Research Letters*, *47*, e2020GL090041. https://doi.org/10.1029/2020GL090041

Received 29 JUL 2020
Accepted 24 SEP 2020
Accepted article online 30 SEP 2020

©2020. American Geophysical Union. All Rights Reserved.

1. Introduction

The outbreak of the Coronavirus Disease 2019 (COVID-19) in early 2020 had tremendous social and economic impacts on China (Tian et al., 2020; C. Wang, Horby, et al., 2020; Zu et al., 2020). The Chinese government imposed an unpreceded nationwide mandatory lockdown to contain its spread shortly after its first occurrence. As the early epicenter, the first lockdown was implemented in Wuhan on 23 January. Following that, all other major cities went into lockdown after the Lunar New Year (LNY). Despite differences in local measures, strict COVID lockdowns (CLDs) lasted for at least 3 weeks nationwide. During the CLD period, commercial activities, traffic, and travel were restricted, leading to a substantial reduction in emissions of primary air pollution.

As expected, anthropogenic emissions declined considerably during the CLD period. For instance, the Ozone Monitoring Instrument observed a 48% drop in tropospheric column densities of NO_2 over eastern China during the CLD (Liu et al., 2020). Also reported was a similar decrease in tropospheric NO_2 columns from analyses of TROPOspheric Monitoring Instrument data (Bauwens et al., 2020; Shi & Brasseur, 2020). However, surface aerosol loading did not have a similar reduction despite the substantial decrease in primary pollutant emissions (P. Wang, Chen, et al., 2020). There were episodes of severe air pollution in northern China during the CLD (Le et al., 2020; Sun et al., 2020), incurring a public outcry questioning the effects of the drastic emission control measures implemented in China that could have adverse impacts on the financial well-being in some sectors.

This apparent paradox drew immediate attention to the scientific community who has come up with various sound explanations/hypotheses, one of which was attributed to the formation of secondary pollution (Chang et al., 2020; Huang et al., 2020). While enhanced secondary pollution may play a significant role in the severe air pollution during the CLD, it remains an open question as to if it was the only major factor. If not, what are other factors and their contributions to the severe haze event with the concentrations of atmospheric particulate matter (PM) with diameters less than 2.5 μm ($PM_{2.5}$) more than 100 μg m^{-3}? Le et al. (2020) employed reanalysis data and model simulations in an attempt to attribute the severe air pollution to meteorology and heterogeneous chemistry. However, reanalysis data have considerable uncertainties, especially in the treatment of physical processes in the planetary boundary layer (PBL) (Alapaty

et al., 1997). The PBL height (PBLH), one of the most fundamental PBL quantity, is not modeled accurately (e.g., Banks et al., 2015; Chu et al., 2019; Guo et al., 2016; Su et al., 2017). More importantly, PBLH is associated with aerosol vertical mixing, affecting the concentration of air pollutions emitted near the surface through various interactions and feedback mechanisms (Dong et al., 2017; Lou et al., 2019; Su et al., 2018; Wang et al., 2013).

To quantify the role of the PBL on the severe haze episode that occurred during the CLD, we employed a nationwide PBLH database along with other observations of pollutants and surface meteorological parameters. The abnormally shallow PBL occurring in northern China could account for the unexpected severe air pollution episode, which likely offset the reduction in primary emissions. The incident serves as a natural test bed for understanding aerosol-PBL interactions in a historically low-emission scenario.

2. Data and Methods

2.1. Data Sets

In this study, we acquired the data from 1,138 environmental stations and 55 radiosonde stations in eastern China. Figure S1 in the supporting information shows the topography and locations of stations. Measured routinely at the environmental stations are carbon monoxide (CO), sulfur dioxide (SO_2), nitrogen dioxide (NO_2), and $PM_{2.5}$ concentrations at 1-hr intervals, released to the public with sound quality (Liang et al., 2016; Wei et al., 2019, 2020). The China Meteorological Administration is responsible for maintaining the radiosonde stations, in which the vertical profiles of pressure, water vapor, temperature, and wind are routinely measured at 08:00 and 20:00 Beijing Time (BJT = UTC + 8), as well as at 1400 BJT during summer only. The original resolution of radiosonde data varies with the ascending height of the balloon (Guo et al., 2016; Zhang et al., 2018), unified to a fixed resolution of 5 hPa (Liu & Liang, 2010). At the radiosonde sites, hourly measurements of meteorological variables also are available at the surface level (Guo et al., 2017, 2019). Given the availability of both environmental and meteorological data, valid data periods are 2013–2020 in Beijing and 2016–2020 in other places. In this study, we employ the daily means of environmental and meteorological quantities, averaged over 0800–1900 BJT, when most commercial activities and transport sectors were suppressed during the CLD.

2.2. Determination of PBLH

Radiosonde-measured temperature and pressure profiles determined the vertical profiles of potential temperature. Since radiosonde soundings were not available at noon, we adopted the parcel method proposed by Holzworth (1964). This widely used method continuously tracks PBLHs, based on a morning radiosonde sounding combined with daily meteorological data (Karimian et al., 2016; Li et al., 2020; Zhang et al., 2014).

Due to the overshooting of rising parcels, the potential temperature at PBL top is generally higher than the surface value (Liu & Liang, 2010). Therefore, we modified the parcel method by adding a threshold. Assuming that surface temperatures increase during the morning, the parcel method also assumes that an air parcel is lifted adiabatically from the near surface to the upper part of PBL and keeps an approximately constant potential temperature. Following the idea of 1.5-θ-increase method (Nielsen-Gammon et al., 2008), a threshold of 1.5 K is added to the original method. The upper boundary of PBL is thus defined as the height where the environmental potential temperature first exceeds the current surface potential temperature by more than 1.5 K. In particular, the environmental potential temperature profile is determined by the radiosonde launched at 0800 BJT at radiosonde sites, while the surface potential temperature is obtained from surface-based meteorological measurements.

Note that the PBL undergoes regime transition in a diurnal cycle. It typically transforms from a stable boundary layer to a neutral or convective boundary layer during the day and then becomes a stable boundary layer again at night. Due to this diurnal feature, we only retrieve the noontime PBL, which is well developed and most representative of daily development due to the strong turbulent mixing (Stull, 1988; Yang et al., 2013). Hereafter, we define the noontime as 1100–1500 BJT. Among the 55 sites considered, 53 of them have continuous 4-year records of PBLH (2016–2020).

The assumptions made in the parcel method will lead to some biases in the estimation of the PBLH. Regarding this issue, we evaluated the noontime PBLH derived from the parcel method through comparisons with those calculated using real-time radiosonde data from 1400 BJT in Beijing during the summer

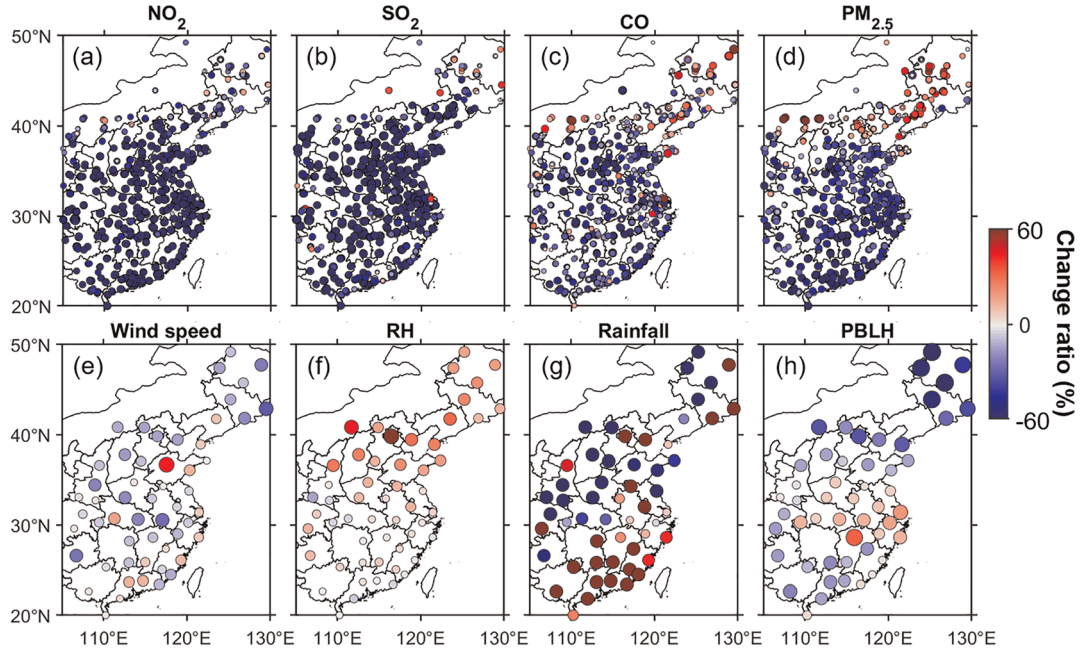


Figure 1. Percentage differences in (a) NO_2, (b) SO_2, (c) CO, (d) $PM_{2.5}$, (e) wind speed (WS), (f) relative humidity (RH), (g) rainfall amount, and (h) planetary boundary layer height (PBLH) between mean values during the COVID-19 lockdown (26 January to 17 February 2020) and the climatological mean during the same period of the years 2016 to 2019. The PBLH is retrieved during noontime (1100–1500 Beijing Time, or BJT) due to the diurnal transition, while other parameters are averaged during daytime (0800–1900 BJT).

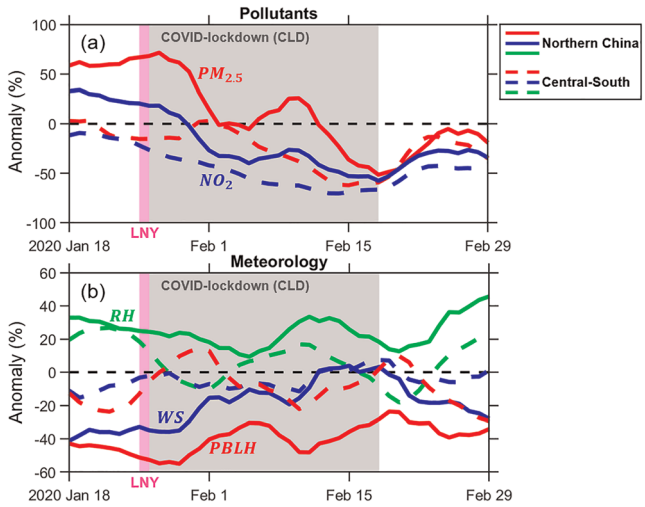


Figure 2. (a) $PM_{2.5}$ (red line) and NO_2 (blue line) anomalies and (b) planetary boundary layer height (PBLH, red line), wind speed (WS, blue line), and relative humidity (RH, green line) anomalies over China. In (a) and (b), a 9-day smoothing window was applied to all anomalies. Colored solid lines represent results averaged over northern China (latitudes above 38°N), and colored dashed lines represent results averaged over central and southern China (latitudes below 38°N). Zero lines represent the climatology averaged over the same COVID lockdown (CLD) period of the years 2016 to 2019. Pink areas represent the Lunar New Year (LNY), and gray areas represent the CLD period.

(Figure S2). The PBLHs derived from the parcel method agree well with those derived from the 1.5-θ-increase method or the Liu and Liang (2010) method, with high correlation coefficients (~0.8).

3. Results

3.1. Nationwide Changes in Air Pollution and Meteorology

We focus on the CLD, defined as the period between 26 January and 17 February 2020, when anthropogenic emissions dramatically declined (Huang et al., 2020; Liu et al., 2020). We compared the surface pollutant-concentrations with climatological means for the same period. Hereafter, climatological means refer to the same period in the Chinese lunar calendar but from 2016 to 2019 to potentially account for the holiday effect (Le et al., 2020; Zhang et al., 2010). Figure 1 presents the ratios of changes in NO_2, SO_2, CO, and $PM_{2.5}$. On average, surface concentrations of NO_2, SO_2, and CO decreased by 45%, 47%, and 20%, respectively. The reduced primary emissions directly lead to the dramatic decrease in gaseous pollution. Moreover, despite the considerable reduction in emissions during the CLD, $PM_{2.5}$ increased by 19% in the northern part of China, with large regional discrepancies (Figure 1d).

Figures 1e–1h show simultaneous changes in meteorological variables (i.e., wind speed [WS], relative humidity [RH], rainfall amount, and PBLH). In general, WS exhibited a 0–10% decrease during the CLD period, except for a few increasing trends. RH did not notably change in southern China but considerably increased in northern China on the order of a

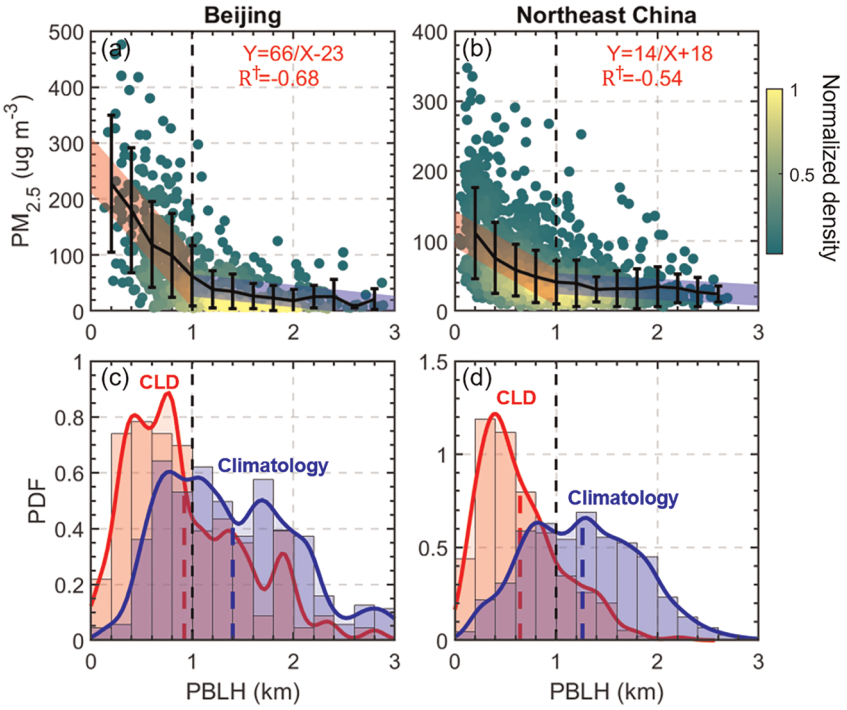


Figure 3. The relationship between the planetary boundary layer height (PBLH) and $PM_{2.5}$ over (a) Beijing and (b) northeast China during wintertime. The black dots and whiskers represent average values and standard deviations in each bin, respectively. The vertical black dashed line shows the turning point of the PBLH (1 km). The thick red lines and thick blue lines indicate regressions before and after the turning point, respectively. The fitting functions and coefficient correlations of the inverse fittings are given at the top of each panel. Red and blue areas in panels (c) and (d) represent the probability density functions (PDFs) of the PBLH during the COVID lockdown (CLD) and the climatology, respectively. The red and blue dash lines represent the mean PBLH during the CLD and the climatological mean, respectively.

mean of 25% and a range of 10–70%. A moist environment would facilitate the formation of secondary aerosols (Wang et al., 2016). Rainfall is unlikely a major driving force behind the spatial pattern of air pollutants because both southern and northern China generally experienced more precipitation during the CLD to varying degrees. By contrast, the PBLH showed dramatic changes: significant decreases during the CLD in northern China but increases in central China. Meanwhile, the changes in surface temperature are similar to the changes in PBL to some extent (Figure S3). Shallow PBL is generally associated with the low surface temperature.

Regional differences in the ratios of changes in pollutants and meteorology are notable, especially the sharp contrast between northern China (latitudes above 38°N) and central/southern China (latitudes below 38°N). We averaged the $PM_{2.5}$, NO_2, PBLH, WS, and RH anomalies during the CLD within each region, and all anomalies are normalized by climatological means: (values in 2020 − Climatology)/Climatology. Figure 2a reveals that the gaseous pollution diminished considerably during the CLD, presumably as a result of the lockdown, and gradually recovered to normal levels after the CLD. Near the end of the CLD, NO_2 and $PM_{2.5}$ both decreased by more than 50% in different parts of China. In particular, over central and southern China, $PM_{2.5}$ generally decreased by 30%, and NO_2 decreased by 50% during the CLD. However, this was not the case in northern China where $PM_{2.5}$ concentrations were higher than normal. This is linked to meteorological conditions (Figure 2b). In northern China, both the humid environment and low WSs during the CLD favored the formation and accumulation of aerosols. The PBLH in northern China had the most significant decrease, that is, a 45% decrease. In central/southern China, changes in these meteorological variables were in similar directions but with lesser magnitudes. Comparing the change ratios in northern China to those in central/southern China, WS was 9.7% lower, RH was 19.8%

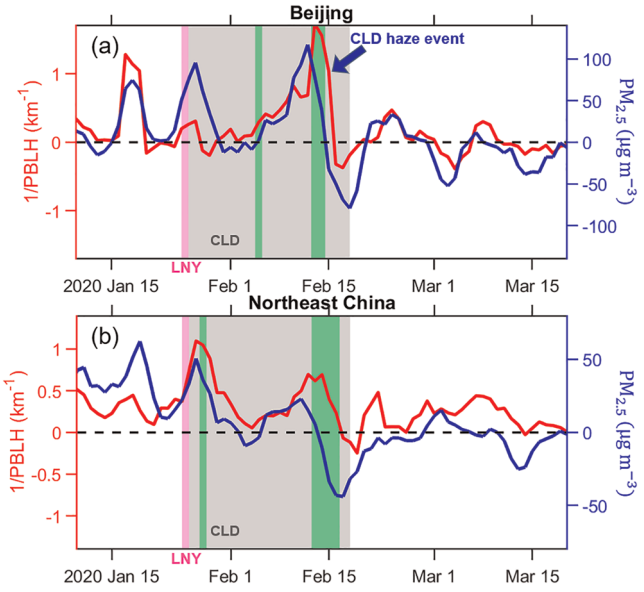


Figure 4. Time series of 1/PBLH (planetary boundary layer height, red lines) and $PM_{2.5}$ (blue lines) over (a) Beijing and (b) northeast China, with a 3-day smoothing window. Seasonal cycles, trends, and climatology have been removed in the time series. Pink areas represent the Lunar New Year (LNY), and gray areas represent the COVID lockdown (CLD) period. The green areas indicate the periods with daily rainfall above 1 mm. A notable haze event that occurred in Beijing during the CLD is pointed out in (a).

higher, and the PBLH was 39.1% lower. The PBLH could play a more dominant role in enhancing air pollution during the CLD, discussed next.

3.2. Synergistic Changes in the PBLH and $PM_{2.5}$ Concentration

Because northern China experienced an unusual increase in $PM_{2.5}$ levels during the CLD, we investigated two regions of interests: Beijing and northeast China (Figure S1). Table S1 lists the radiosonde stations in these two regions. Data from environmental and radiosonde stations are matched if the stations are located within 25 km of each other. Figures 3a and 3b show the general relationships between PBLH and $PM_{2.5}$ during wintertime in Beijing and northeast China. Following Su et al. (2018), an inverse function (i.e., $f(x) = {}^{A}/_{x} + B$) describes the relationship between PBLH and $PM_{2.5}$ (more details are given in the supporting information). During wintertime, the relationship was highly nonlinear. The $PM_{2.5}$ concentration increased rapidly with decreasing PBLH for PBLHs lower than 1 km. This dependence weakened for higher PBLHs. Although it is not an absolute value, 1 km appears to be the turning point dictating the $PM_{2.5}$-PBLH relationship.

To gain further insight into the potential role of the PBL in regulating air pollution during the CLD, we compared the probability density functions of the PBLH during the CLD with that during the same period in the lunar calendar during the previous 4 years. The PBLH was much lower in both Beijing and northeast China during the CLD compared with the mean of the previous 4 years. The frequency of PBLHs lower than the turning point was significantly higher during the CLD. According to the climatology, the PBLH was mostly above the turning point, corresponding to a weak interaction scenario. The shallow-PBL cases during the CLD appear to have triggered a strong aerosol-PBL interaction, leading to excessively high near-surface aerosol loadings. Due to the positive feedback loop (Bond et al., 2013; Ding et al., 2016; Petäjä et al., 2016; Su et al., 2020; Z. Li et al., 2017), the low-PBL effect amplified, contributing to the drastic changes in $PM_{2.5}$ when the PBLH was below the turning point.

Figure 4 shows the time series of normalized $PM_{2.5}$ and 1/PBLH in Beijing and northeast China. The normalization is done by subtracting the monthly mean, removing the trend, and subtracting the mean value in the lunar calendar. Highly consistent changes in 1/PBLH and $PM_{2.5}$ are found in the two regions. The $PM_{2.5}$ concentration was higher than normal during the CLD in both Beijing and northeast China, which is associated with the increase in 1/PBLH. Note that there are some discrepancies between the time series of $PM_{2.5}$ and PBLH. The precipitation effectively reduced the pollution level at the end of CLD haze event. Meanwhile, PBLH still maintains the relatively low values due to the suppressed surface fluxes. Therefore, a decrease in $PM_{2.5}$ is ahead of the decrease in 1/PBLH during the CLD haze event. In addition, the relationships between meteorological factors and $PM_{2.5}$ are established, following standardized multiple regressions whose coefficients denote the relative importance of the individual factors (Table S2). PBLH turns out to have the strongest partial correlation with the daily $PM_{2.5}$ concentration. The other factors also matter.

In the middle of the CLD, Beijing experienced a heavy haze episode. Table S3 lists the daily air pollution and meteorological parameters during the CLD. During the CLD haze event, there were five consecutive days with noontime PBLHs lower than 0.7 km, which is rare, having only occurred three times during winter from 2013 to 2019 (detailed in Table S3). For other shallow PBL periods in the previous 7 years, the mean $PM_{2.5}$ is 270 μg m^{-3}, with a standard deviation of 125 μg m^{-3}. A continuously low PBLH can generate an unfavorable environment for the dissipation of pollutants, thus compounding severe air pollution in Beijing.

Further investigated were historical cases with similar meteorological conditions in Beijing, as detailed in the supporting information. Figure 5 presents the distribution of daytime $PM_{2.5}$ under these similar conditions. Even though WS and RH during the CLD favored the accumulation of near-surface pollutants, these conditions did not necessarily lead to a high surface $PM_{2.5}$ concentration. Due to the unprecedented

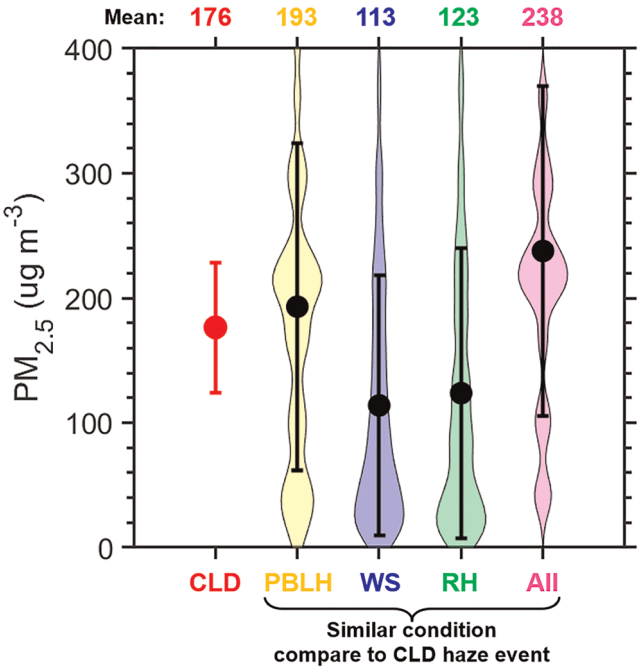


Figure 5. The red dot and whisker represent the average value and standard deviation of daytime $PM_{2.5}$ during the COVID lockdown (CLD) haze event in Beijing. Based on wintertime data from 2013 to 2019, days with a similar planetary boundary layer height (PBLH), wind speed (WS), relative humidity (RH), and all three are selected (less than 20% difference). The distribution of daytime $PM_{2.5}$ is presented under these similar conditions. The black dot and whisker represent the average value and standard deviation, while the width of the color-shaded areas represents the smoothed distribution of daytime $PM_{2.5}$. The mean $PM_{2.5}$ values for these categories are given at the top of the figure (unit: $\mu g\ m^{-3}$).

reduction of various emissions during the CLD, the $PM_{2.5}$ level appears to be the lowest scenario compared with the previous level under similar meteorological conditions.

The abnormally shallow PBL during the CLD haze event is attributed to atmospheric dynamics. Using Modern-Era Retrospective analysis for Research and Applications Version 2 reanalysis data (Gelaro et al., 2017), we examine the composite mean meteorological field during the CLD haze event in Figure S4. During this period, Beijing is located near the southeast flank of a low-pressure system. The southwesterly winds advected warm air masses over the cold surface, which stabilized the PBL. This process is commonly known as the mechanism behind formations of frontal inversion (Zhang et al., 2009). The dynamic processes caused a heating effect on the upper PBL and a cooling effect near the surface during this period (Figure S5), notably reducing the PBLH. This is also consistent with previous studies showing the frequent occurrences of more stable PBLs under similar synoptic patterns (e.g., Miao et al., 2017; Wu et al., 2017).

4. Conclusions

The nationwide lockdown of economic activities in China provided a unique opportunity to differentiate the impact of emissions and meteorology on severe air pollution episodes that occurred in northern China. To date, reported findings have chiefly focused on the role of secondary aerosols. Using comprehensive ground-based observations of air pollutants, PBLH, and other meteorological variables, we argue that the abnormally shallow PBL during the CLD was likely a key player in dictating $PM_{2.5}$ in northern China.

Compared with the climatology during the same period in the previous 4 years, the noontime PBLH in central China increased during the CLD but decreased by more than 40% in northern China, triggering a strong aerosol-PBL interaction. As the most prominent city in northern China, Beijing experienced a persistent low PBLH during the CLD, leading to a severely polluted episode relative to historical data. In addition to the effects of PBL, secondary aerosols may further exacerbate surface pollution (Huang et al., 2020; Le et al., 2020; Sun et al., 2020).

The in-depth observation-based analysis presented here may help explain the high-profile haze event that occurred in Beijing during the CLD. The aerosol-PBL interaction was likely a key mechanism behind the severe pollution in northern China, given the exceptionally low-emission scenario. This may resolve the paradox of the well-established relationship between air pollution and primary emissions during this special period. In the long run, however, emissions remain a critical factor in driving the variation in $PM_{2.5}$.

Data Availability Statement

MERRA-2 reanalysis data can be found online at (https://disc.gsfc.nasa.gov/datasets/M2I1NXASM_5.12.4/summary?keywords=merra2). Hourly air pollution measurements are released by the Ministry of Ecology and Environment of China (https://aqicn.org/data-platform/covid19/). Surface meteorological data and radiosonde are provided by the China Meteorological Data Service Center of the China Meteorological Administration (http://data.cma.cn/en/?r=data/detail&dataCode=B.0011.0001C). The data sets can be found on these websites or request from the lead author (tianning@umd.edu).

Acknowledgments

This study is supported by the National Science Foundation (AGS1837811) and the National Key R&D Program of China (2017YFC1501702). We appreciate the provision of meteorological and radiosonde measurements by the China Meteorological Administration and for the provision of air pollution measurements by the Ministry of Ecology and Environment of China. We sincerely thank the MERRA team for their data sets.

References

Alapaty, K., Pleim, J. E., Raman, S., Niyogi, D. S., & Byun, D. W. (1997). Simulation of atmospheric boundary layer processes using local- and nonlocal-closure schemes. *Journal of Applied Meteorology*, *36*(3), 214–233. https://doi.org/10.1175/1520-0450(1997)036<0214:SOABLP>2.0.CO;2

Banks, R. F., Tiana-Alsina, J., Rocadenbosch, F., & Baldasano, J. M. (2015). Performance evaluation of the boundary-layer height from lidar and the Weather Research and Forecasting model at an urban coastal site in the north-east Iberian Peninsula. *Boundary-Layer Meteorology*, *157*(2), 265–292. https://doi.org/10.1007/s10546-015-0056-2

Bauwens, M., Compernolle, S., Stavrakou, T., Müller, J.-. F., van Gent, J., Eskes, H., et al. (2020). Impact of coronavirus outbreak on NO_2 pollution assessed using TROPOMI and OMI observations. *Geophysical Research Letters*, *47*, e2020GL087978. https://doi.org/10.1029/2020GL087978

Bond, T. C., Doherty, S. J., Fahey, D. W., Forster, P. M., Berntsen, T., DeAngelo, B. J., et al. (2013). Bounding the role of black carbon in the climate system: A scientific assessment. *Journal of Geophysical Research: Atmospheres*, *118*, 5380–5552. https://doi.org/10.1002/jgrd.50171

Chang, Y., Huang, R. J., Ge, X., Huang, X., Hu, J., Duan, Y., et al. (2020). Puzzling haze events in China during the coronavirus (COVID-19) shutdown. *Geophysical Research Letters*, *47*, e2020GL088533. https://doi.org/10.1029/2020GL088533

Chu, Y., Li, J., Li, C., Tan, W., Su, T., & Li, J. (2019). Seasonal and diurnal variability of planetary boundary layer height in Beijing: Intercomparison between MPL and WRF results. *Atmospheric Research*, *227*, 1–13. https://doi.org/10.1016/j.atmosres.2019.04.017

Ding, A. J., Huang, X., Nie, W., Sun, J. N., Kerminen, V. M., Petäjä, T., et al. (2016). Enhanced haze pollution by black carbon in megacities in China. *Geophysical Research Letters*, *43*, 2873–2879. https://doi.org/10.1002/2016GL067745

Dong, Z., Li, Z., Yu, X., Cribb, M., Li, X., & Dai, J. (2017). Opposite long-term trends in aerosols between low and high altitudes: A testimony to the aerosol-PBL feedback. *Atmospheric Chemistry and Physics*, *17*(12), 7997–8009. https://doi.org/10.5194/acp-17-7997-2017

Gelaro, R., McCarty, W., Suárez, M. J., Todling, R., Molod, A., Takacs, L., et al. (2017). The Modern-Era Retrospective Analysis for Research and Applications, Version 2 (MERRA-2). *Journal of Climate*, *30*(14), 5419–5454. https://doi.org/10.1175/JCLI-D-16-0758.1

Guo, J., Miao, Y., Zhang, Y., Liu, H., Li, Z., Zhang, W., et al. (2016). The climatology of planetary boundary layer height in China derived from radiosonde and reanalysis data. *Atmospheric Chemistry and Physics*, *16*(20), 13,309–13,319.

Guo, J., Su, T., Chen, D., Wang, J., Li, Z., Lv, Y., et al. (2019). Declining summertime local-scale precipitation frequency over China and the United States, 1981–2012: The disparate roles of aerosols. *Geophysical Research Letters*, *46*, 13,281–13,289. https://doi.org/10.1029/2019GL085442

Guo, J., Su, T., Li, Z., Miao, Y., Li, J., Liu, H., et al. (2017). Declining frequency of summertime local-scale precipitation over eastern China from 1970 to 2010 and its potential link to aerosols. *Geophysical Research Letters*, *44*, 5700–5708. https://doi.org/10.1002/2017GL073533

Holzworth, G. C. (1964). Estimates of mean maximum mixing depths in the contiguous United States. *Monthly Weather Review*, *92*(5), 235–242. https://doi.org/10.1175/1520-0493(1964)092<0235:EOMMMD>2.3.CO;2

Huang, X., Ding, A., Gao, J., Zheng, B., Zhou, D., Qi, X., et al. (2020). Enhanced secondary pollution offset reduction of primary emissions during COVID-19 lockdown in China. *National Science Review*. https://doi.org/10.1093/nsr/nwaa137

Karimian, H., Li, Q., Li, C., Jin, L., Fan, J., & Li, Y. (2016). An improved method for monitoring fine particulate matter mass concentrations via satellite remote sensing. *Aerosol and Air Quality Research*, *16*(4), 1081–1092. https://doi.org/10.4209/aaqr.2015.06.0424

Le, T., Wang, Y., Liu, L., Yang, J., Yung, Y. L., Li, G., & Seinfeld, J. H. (2020). Unexpected air pollution with marked emission reductions during the COVID-19 outbreak in China. *Science*, *369*(6504), 702–706. https://doi.org/10.1126/science.abb7431

Li, J., Chu, Y., Li, X., & Dong, Y. (2020). Long-term trends of global maximum atmospheric mixed layer heights derived from radiosonde measurements. *Environmental Research Letters*, *15*(3), 034054. https://doi.org/10.1088/1748-9326/ab7952

Li, Z., Guo, J., Ding, A., Liao, H., Liu, J., Sun, Y., et al. (2017). Aerosol and boundary-layer interactions and impact on air quality. *National Science Review*, *4*(6), 810–833. https://doi.org/10.1093/nsr/nwx117

Liang, X., Li, S., Zhang, S., Huang, H., & Chen, S. X. (2016). $PM_{2.5}$ data reliability, consistency, and air quality assessment in five Chinese cities. *Journal of Geophysical Research: Atmospheres*, *121*, 10,220–10,236. https://doi.org/10.1002/2016JD024877

Liu, F., Page, A., Strode, S. A., Yoshida, Y., Choi, S., Zheng, B., et al. (2020). Abrupt decline in tropospheric nitrogen dioxide over China after the outbreak of COVID-19. *Science Advances*, *6*(28), eabc2992.

Liu, S., & Liang, X. Z. (2010). Observed diurnal cycle climatology of planetary boundary layer height. *Journal of Climate*, *23*(21), 5790–5809. https://doi.org/10.1175/2010JCLI3552.1

Lou, M., Guo, J., Wang, L., Xu, H., Chen, D., Miao, Y., et al. (2019). On the relationship between aerosol and boundary layer height in summer in China under different thermodynamic conditions. *Earth and Space Science*, *6*, 887–901. https://doi.org/10.1029/2019EA000620

Miao, Y., Guo, J., Liu, S., Liu, H., Li, Z., Zhang, W., & Zhai, P. (2017). Classification of summertime synoptic patterns in Beijing and their associations with boundary layer structure affecting aerosol pollution. *Atmospheric Chemistry and Physics*, *17*(4), 3097–3110. https://doi.org/10.5194/acp-17-3097-2017

Nielsen-Gammon, J. W., Powell, C. L., Mahoney, M. J., Angevine, W. M., Senff, C., White, A., et al. (2008). Multisensor estimation of mixing heights over a coastal city. *Journal of Applied Meteorology and Climatology*, *47*(1), 27–43. https://doi.org/10.1175/2007JAMC1503.1

Petäjä, T., Järvi, L., Kerminen, V. M., Ding, A. J., Sun, J. N., Nie, W., et al. (2016). Enhanced air pollution via aerosol-boundary layer feedback in China. *Scientific Reports*, *6*(1), 18998. https://doi.org/10.1038/srep18998

Shi, X., & Brasseur, G. (2020). The response in air quality to the reduction of Chinese economic activities during the COVID-19 outbreak. *Geophysical Research Letters*, *47*, e2020GL088070. https://doi.org/10.1029/2020GL088070

Stull, R. B. (1988). *An introduction to boundary layer meteorology*. Dordrecht: Springer Netherlands. https://doi.org/10.1007/978-94-009-3027-8

Su, T., Li, J., Li, C., Xiang, P., Lau, A. K. H., Guo, J., et al. (2017). An intercomparison of long-term planetary boundary layer heights retrieved from CALIPSO, ground-based lidar, and radiosonde measurements over Hong Kong. *Journal of Geophysical Research: Atmospheres*, *122*, 3929–3943. https://doi.org/10.1002/2016JD025937

Su, T., Li, Z., & Kahn, R. (2018). Relationships between the planetary boundary layer height and surface pollutants derived from lidar observations over China: Regional pattern and influencing factors. *Atmospheric Chemistry and Physics*, *18*(21), 15,921–15,935. https://doi.org/10.5194/acp-18-15921-2018

Su, T., Li, Z., Li, C., Li, J., Han, W., Shen, C., et al. (2020). The significant impact of aerosol vertical structure on lower atmosphere stability and its critical role in aerosol-planetary boundary layer (PBL) interactions. *Atmospheric Chemistry and Physics*, *20*(6), 3713–3724. https://doi.org/10.5194/acp-20-3713-2020

Sun, Y., Lei, L., Zhou, W., Chen, C., He, Y., Sun, J., et al. (2020). A chemical cocktail during the COVID-19 outbreak in Beijing, China: Insights from six-year aerosol particle composition measurements during the Chinese New Year holiday. *Science of the Total Environment*, *742*, 140739. https://doi.org/10.1016/j.scitotenv.2020.140739

Tian, H., Liu, Y., Li, Y., Wu, C. H., Chen, B., Kraemer, M. U., et al. (2020). An investigation of transmission control measures during the first 50 days of the COVID-19 epidemic in China. *Science*, *368*(6491), 638–642. https://doi.org/10.1126/science.abb6105

Wang, C., Horby, P. W., Hayden, F. G., & Gao, G. F. (2020). A novel coronavirus outbreak of global health concern. *Lancet*, *395*, 496–496.
Wang, G., Zhang, R., Gomez, M. E., Yang, L., Zamora, M. L., Hu, M., et al. (2016). Persistent sulfate formation from London fog to Chinese haze. *Proceedings of the National Academy of Sciences*, *113*(48), 13,630–13,635. https://doi.org/10.1073/pnas.1616540113
Wang, P., Chen, K., Zhu, S., Wang, P., & Zhang, H. (2020). Severe air pollution events not avoided by reduced anthropogenic activities during COVID-19 outbreak. *Resoures, Conservation, and Recycling*, *158*, 104814. https://doi.org/10.1016/j.resconrec.2020.104814
Wang, Y., Khalizov, A., Levy, M., & Zhang, R. (2013). New directions: Light-absorbing aerosols and their atmospheric impacts. *Atmospheric Environment*, *81*, 713–715. https://doi.org/10.1016/j.atmosenv.2013.09.034
Wei, J., Li, Z., Cribb, M., Huang, W., Xue, W., Sun, L., et al. (2020). Improved 1 km resolution $PM_{2.5}$ estimates across China using enhanced space–time extremely randomized trees. *Atmospheric Chemistry and Physics*, *20*(6), 3273–3289. https://doi.org/10.5194/acp-20-3273-2020
Wei, J., Li, Z., Guo, J., Sun, L., Huang, W., Xue, W., et al. (2019). Satellite-Derived 1-km-Resolution PM1 Concentrations from 2014 to 2018 across China. *Environmental Science & Technology*, *53*(22), 13,265–13,274. https://doi.org/10.1021/acs.est.9b03258
Wu, P., Ding, Y., & Liu, Y. (2017). Atmospheric circulation and dynamic mechanism for persistent haze events in the Beijing-Tianjin-Hebei region. *Advances in Atmospheric Sciences*, *34*(4), 429–440. https://doi.org/10.1007/s00376-016-6158-z
Yang, D. W., Li, C. C., Lau, A. K. H., & Li, Y. (2013). Long-term measurement of daytime atmospheric mixing layer height over Hong Kong. *Journal of Geophysical Research: Atmospheres*, *118*, 2422–2433. https://doi.org/10.1002/jgrd.50251
Zhang, M., Wang, X., Chen, J., Cheng, T., Wang, T., Yang, X., et al. (2010). Physical characterization of aerosol particles during the Chinese New Year's firework events. *Atmospheric Environment*, *44*(39), 5191–5198. https://doi.org/10.1016/j.atmosenv.2010.08.048
Zhang, Q., Ma, X., Tie, X., Huang, M., & Zhao, C. (2009). Vertical distributions of aerosols under different weather conditions: Analysis of in-situ aircraft measurements in Beijing, China. *Atmospheric Environment*, *43*(34), 5526–5535. https://doi.org/10.1016/j.atmosenv.2009.05.037
Zhang, W., Guo, J., Miao, Y., Liu, H., Song, Y., Fang, Z., et al. (2018). On the summertime planetary boundary layer with different thermodynamic stability in China: A radiosonde perspective. *Journal of Climate*, *31*(4), 1451–1465. https://doi.org/10.1175/JCLI-D-17-0231.1
Zhang, Y., Gao, Z., Li, D., Li, Y., Zhang, N., Zhao, X., & Chen, J. (2014). On the computation of planetary boundary-layer height using the bulk Richardson number method. *Geoscientific Model Development*, *7*(6), 2599–2611. https://doi.org/10.5194/gmd-7-2599-2014
Zu, Z. Y., Jiang, M. D., Xu, P. P., Chen, W., Ni, Q. Q., Lu, G. M., & Zhang, L. J. (2020). Coronavirus Disease 2019 (COVID-19): A perspective from China. *Radiology*, 200490.